JOURNAL OF GEOPHYSICAL RESEARCH, VOL. 113, C08029, doi:10.1029/2007JC004455, 2008

Simulated impact of double-diffusive mixing on physical and biogeochemical upper ocean properties

Mirjam S. Glessmer,[1] Andreas Oschlies,[1] and Andrew Yool[2]

Received 19 July 2007; revised 4 April 2008; accepted 6 May 2008; published 16 August 2008.

[1] A global ocean circulation model coupled with a simple marine ecosystem model including the biogeochemical cycles and air–sea fluxes of oxygen and carbon dioxide is used to investigate the impact of double-diffusive mixing on upper ocean physical and biogeochemical properties. By comparing results for two different parameterizations of double-diffusive mixing, we also examine the sensitivity of our estimates to the particular representation of this process in general circulation models. Differences between the two parameterizations considered turned out to be much smaller than the difference with respect to a model run without double-diffusive mixing. For both parameterizations, the impact on upper ocean temperatures and salinities is relatively small (±1°C, ±0.25 psu regionally and 0.04°C, 0.01 psu as global rms difference over the top 50 m) and changes in surface heat flux amount to 0.05 W m^{-2} globally. However primary production and export production in the oligotrophic subtropics are found to increase by up to 80% and 120%, respectively, when double diffusion is switched on in the model. Double-diffusive nutrient supply generates an additional oceanic carbon uptake of about 0.4 g C m^{-2} $year^{-1}$, amounting to 0.14 Gt C $year^{-1}$ globally.

Citation: Glessmer, M. S., A. Oschlies, and A. Yool (2008), Simulated impact of double-diffusive mixing on physical and biogeochemical upper ocean properties, *J. Geophys. Res.*, *113*, C08029, doi:10.1029/2007JC004455.

1. Introduction

[2] Developing an accurate description of mixing in general, and of vertical or diapycnal mixing in particular, is one of the major challenges of current state-of-the-art ocean and climate models [*Griffies et al.*, 2000]. Processes that generate diapycnal mixing in the stratified ocean interior include the breaking of internal waves, Kelvin–Helmholtz shear instabilities, and double diffusion. Here, we focus on double-diffusive mixing and attempt to quantitatively estimate its impact on upper ocean physics and biogeochemistry.

[3] Double-diffusive mixing is caused by different molecular diffusivities of heat and salt. Early realizations of the potential importance of such differences include the studies of *Jevons* [1857] and Stommel's "perpetual salt fountain" [*Stommel et al.*, 1956]. In sea water, the molecular diffusion of heat is much faster, roughly by a factor 100, than that of salt [*Zhang et al.*, 1998]. Under suitable conditions, the faster erosion of temperature gradients compared to salinity gradients on molecular scales can then generate static instabilities and subsequent macroscopic turbulence and mixing.

[4] Double diffusion has been measured in various regions of the ocean as, for example, the lower boundary of the Mediterranean Outflow west of Gibraltar [*Zenk*, 1970], the western tropical North Atlantic [*Schmitt*, 1987], or the Arctic [*Rudels et al.*, 1999; *Timmermans et al.*, 2004].

[5] *You* [2002] deduced from the World Ocean Atlas [*Levitus*, 1994] that as much as 44% of the ocean volume satisfies the necessary conditions for double diffusion. By affecting vertical temperature and salinity profiles, double-diffusive mixing can lead to changes in surface heat fluxes and sea ice thermodynamics, possibly impacting on water mass formation and ocean dynamics. Additionally, double diffusion can act as to reduce anomalies in spiciness and thereby attenuate their possible climatic impacts ([*Johnson*, 2006]).

[6] Double-diffusive mixing is of particular interest for estimates of upper ocean nutrient supply to the subtropical gyres. In a regional modeling study, *Oschlies et al.* [2003] found that salt-finger induced mixing (parameterized after *Zhang et al.* [1998]) generated nutrient fluxes comparable to those associated with mechanically-induced turbulence or with mesoscale eddies. Applying the same mixing parameterization to hydrographic measurements in the subtropical North Atlantic, *Dietze et al.* [2004] inferred that nutrient transport into the nutrient-consuming surface layer by salt fingering was more than fivefold higher than transport due to internal-wave induced turbulence.

[7] The aim of the present paper is to give a first quantitative estimate of the global impact of double diffusion on upper ocean properties. As a complete mechanistic

[1]IFM-GEOMAR, Leibniz Institute of Marine Sciences at Kiel University, Kiel, Germany.
[2]Ocean Modelling and Forecasting, National Oceanography Centre, Southampton, UK.

0148-0227/08/2007JC004455$09.00

understanding of the amount of macroscopic mixing generated by double diffusion is not yet available, we employ two different empirical parameterizations of double-diffusive mixing. These are introduced into a global general circulation model coupled with a simple nutrient–phytoplankton–zooplankton–detritus (NPZD) ecosystem model together with the biogeochemical cycles of carbon and oxygen, including air–sea gas exchange. The paper is organized as follows: in the following section, we present the model used in this study and describe the different parameterizations of double-diffusive mixing. In section 3, the model results are validated against measurements. Model results are presented and discussed in section 4.1 with a focus on physics, in section 4.2 with focus on biogeochemistry and in section 4.3 with a focus on air–sea fluxes of CO_2 and O_2. The last section summarizes and discusses our conclusions and in an appendix the parameterizations of double-diffusive mixing used in this study are presented in more detail.

2. Methods

2.1. Model

[8] The model used in this study is the Ocean Circulation and Climate Advanced Modelling Project (OCCAM) [*Coward and de Cuevas*, 2005; *Sinha and Yool*, 2006], a primitive equation finite difference ocean general circulation model based on the Geophysical Fluid Dynamics Laboratory's Modular Ocean Model (MOM) version of the Bryan-Cox-Semtner ocean model, here used in a 1° by 1° horizontal resolution. In the vertical there are 66 depth levels, 14 in the top 100 m and 29 in the uppermost 500 m. The maximum depth is 6470 m, and seafloor grid cells assume a fractional size to better represent bathymetry. The sea-ice model is described in detail in *Aksenov* [2002], its thermodynamics are based on *Semtner* [1976], and the dynamics on the elastic-viscous-plastic rheology of *Hunke and Dukowicz* [1997]. OCCAM is forced by surface fluxes of radiative, sensible and latent heat, surface wind stresses, evaporation and precipitation, with a weak relaxation (relaxation time is 30 d) to Levitus monthly sea surface salinity. Relaxing sea surface salinity might act to spuriously sustain the near surface salinity gradient which is being eroded by salt fingering, thereby leading to an overestimation of the salt fingering process, and vice versa in the diffusive layering case. However comparison of E–P between the control run and the double-diffusive runs discussed below suggests that this effect is very small. The surface fluxes are computed from bulk formula that take into account the model's actual sea surface temperature and sea ice cover, with atmospheric conditions taken from the 6 hourly NCEP reanalysis products [*Large et al.*, 1997]. Thus the model can simulate some feedback between the ocean surface and the atmospheric boundary layer and is able to maintain both realistic surface fluxes and sea-surface temperatures.

[9] The biological model is based on the nitrogen-based pelagic ecosystem model of *Oschlies* [2001] to which carbon and oxygen cycles have been added [*Sinha and Yool*, 2006; *Orr et al.*, 1999; *Najjar and Orr*, 1999]. Initial data for nitrate and oxygen were taken from the January fields of the World Ocean Atlas (2001) [*Conkright et al.*, 2002], initial fields for dissolved inorganic carbon (DIC) and alkalinity were derived from GLODAP [*Key et al.*, 2004; *Yool and Sinha*, 2006]. The oceanic DIC field represents the pre-industrial carbon cycle, with the estimated anthropogenic CO_2 subtracted from the total measured GLODAP DIC data [*Key et al.*, 2004]. Pre-industrial carbon simulations were used here to avoid a long, transient simulation under anthropogenic CO_2 forcing.

[10] Three runs were carried out: a "control" run without double diffusion, a run "LMD94" with double diffusion parameterized after *Large et al.* [1994], and a run "ZSH98" with double diffusion parameterized after *Zhang et al.* [1998]. In all experiments, non double-diffusive vertical mixing is parameterized by the K-profile parameterization (KPP, K is the diffusion coefficient) after *Large et al.* [1994], and described as the superposition of several processes. A background value of 0.1×10^{-4} m^2 s^{-1}, representing the mixing due to internal wave activity, is enhanced depending on the local Richardson number (to represent resolved vertical shear) and on surface wind and buoyancy forcing in the mixed layer. All experiments started from the same spun-up state of the physical model corresponding to 2 January 1989. Then, biogeochemical fields were initialized as described above and the experiments were integrated in coupled biogeochemical-physical mode for 16 model years each. While this is not sufficient to reach steady state for the biogeochemical tracers, drifts in the upper ocean properties were everywhere small compared to the seasonal cycle (averaged annual drift in nitrate is 3.9% of the amplitude of the seasonal cycle, 0.1% for DIC and 1.8% for phytoplankton). The model experiments only differ in whether or not double diffusion is switched on and, if it is, which of the two parameterizations of double-diffusive mixing is used.

2.2. Double Diffusion as Function of the Density Ratio

[11] In both parameterizations used here, double-diffusive mixing is parameterized as a function of the density ratio $R_\rho = \frac{\alpha T_Z}{\beta S_Z}$ with thermal expansion coefficient $\alpha = -\frac{1}{\rho}\frac{\delta\rho}{\delta T}$, haline contraction coefficient $\beta = \frac{1}{\rho}\frac{\delta\rho}{\delta S}$, and vertical temperature and salinity gradients $T_Z = \frac{\delta T}{\delta Z}$ and $S_Z = \frac{\delta S}{\delta Z}$, respectively. The density ratio is a measure of the stability of stratification. It describes the relative contributions of the vertical temperature and salinity gradients to the density stratification. The density ratio allows to distinguish different regimes. Two of these are of interest to this study, namely diffusive layering and salt fingering.

[12] Diffusive layering can occur when relatively cold and fresh water overlies warm and salty water, i.e., when the stratification is stable in density ($\alpha T_Z > \beta S_Z$), stable in salt and unstable in temperature ($T_Z < 0$, $S_Z < 0$), hence for a density ratio $0 < R_\rho < 1$. As the molecular diffusivity of salt is about a factor of 100 less than that of temperature, the cold and fresh water directly above the interface will warm faster than it becomes fresh (T and S changes are compared with respect to their impacts on density, αT and βS). Therefore it becomes less dense and rises to a level of its own density. Directly below the interface, the warm and salty water will cool, but largely maintain its salinity, thereby becoming denser. The water will eventually sink to its corresponding density level. As a result, vertical property gradients at the interface are increased.

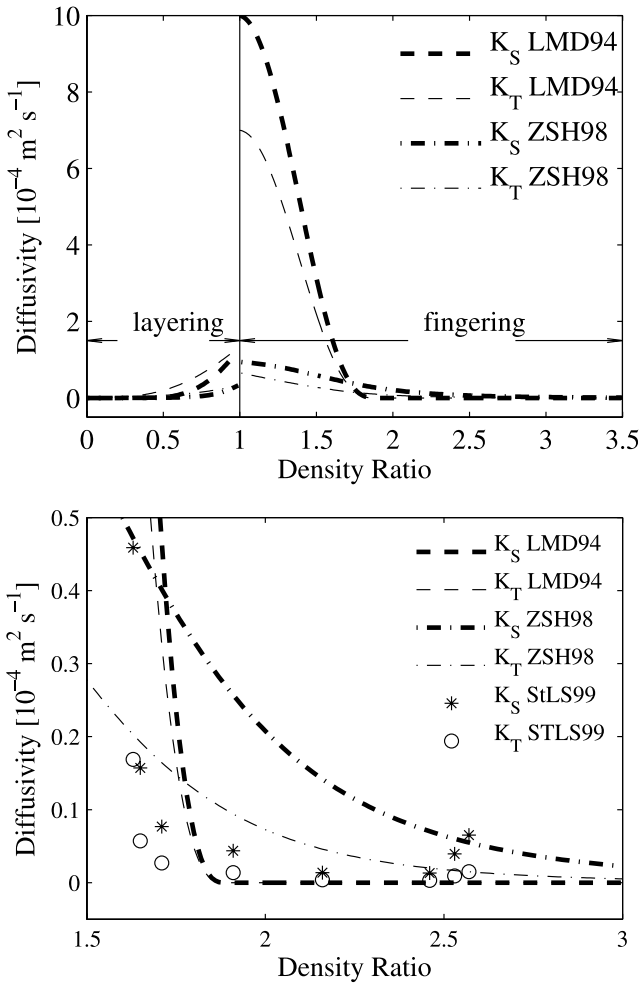

Figure 1. Top: diapycnal diffusivities due to double diffusion, K_T for temperature and K_S for salinity, as a function of the density ratio $R_\rho = \frac{\alpha T_Z}{\beta S_Z}$. A density ratio between 0 and 1 delineates the diffusive layering regime, a density ratio between 1 and 100 (the ratio of the respective molecular diffusivities of temperature and salinity), the salt fingering regime. In the presence of internal waves, salt finger growth rates can lead to significant salt fingering only for density ratios of O(1). The two parameterizations are LMD94 after *Large et al.* [1994], and ZSH98 after *Zhang et al.* [1998]. Bottom: extract of the upper panel with a reduced range of density ratios. StLS99 are estimates made in the NATRE experiment described in *St. Laurent and Schmitt* [1999], K_S and K_T correspond to $k_s^* P^{(f)}$ and $k_\theta^* P^{(f)}$ in their notation, respectively, see Section 3.

[13] Salt fingering can occur when relatively warm, salty water overlies colder and fresher water, i.e., when the stratification is stable in density, stable in temperature and unstable in salinity ($\alpha T_Z > 0$, $\beta S_Z > 0$ and $\alpha T_Z > \beta S_Z$). The water above the interface will cool, while largely maintaining its salinity. Thus it will become denser than the surrounding water and therefore sink until it reaches a level of its own density. The same will happen directly below the interface: water will warm, but remain essentially as fresh as before and hence rise to a level of its own density. These movements occur in long, narrow "fingers"—that have more or less the scale of human fingers–and the process is accordingly called "salt fingering". The net effect of salt fingering is the downward transport of salt across isopycnals and a macroscopic upgradient density flux. The energy required for the mixing is taken out of the salinity stratification. Salt is mixed more effectively than temperature, hence the resulting macroscopic diffusivity of salt is bigger than that of temperature.

[14] Both double-diffusive mixing processes generate so-called staircases in temperature and salinity profiles: nearly homogeneous layers of several meters thickness are separated by thin interfaces with large gradients in both temperature and salinity. These staircases cannot be resolved by the vertical grid of the current model.

2.3. Parameterizations

[15] In this section, the parameterizations are introduced very briefly, for more detail see Figure 1 and Appendix A.

2.3.1. Parameterization LMD94 of Double Diffusive Mixing

[16] Double-diffusive mixing is parameterized after *Large et al.* [1994] in the following way:

[17] (1) Salt Fingering Regime

$$K_s = K_f \left[1 - \left(\frac{R_\rho - 1}{R_\rho^0 - 1}\right)^2\right]^p \text{ for } 1 < R_\rho < R_\rho^0 \quad (1)$$

$$K_s = 0.0 \text{ for } R_\rho \geq R_\rho^0 \quad (2)$$

$$K_\theta = 0.7 K_s \quad (3)$$

where R_ρ is the density ratio described above, K_s is the diffusivity of salt due to double-diffusive mixing, K_θ is the diffusivity of potential temperature due to double-diffusive mixing, $K_f = 10 \times 10^{-4}$ m^2 s^{-1} is the maximum of the diffusivity due to salt fingering, $R_\rho^0 = 1.9$ is the critical density ratio above which mixing because double diffusion is assumed to be not effective, and $p = 3$.

[18] (2) Diffusive Layering Regime

$$K_\theta = 0.909 \times \exp\left(4.6 \times \exp\left[-0.54\left(R_\rho^{-1} - 1\right)\right]\right)\nu \quad (4)$$

with the molecular viscosity $\nu = 1.5 \times 10^{-6}$ m^2 s^{-1}. The diffusivity of salt is

$$K_s = K_\theta\left(1.85 - 0.85 R_\rho^{-1}\right) R_\rho \text{ for } 0.5 \leq R_\rho < 1 \quad (5)$$

$$K_s = K_\theta 0.15 R_\rho \text{ for } R_\rho < 0.5 \quad (6)$$

2.3.2. Parameterization ZSH98 of Double-Diffusive Mixing

[19] Double diffusive mixing is parameterized after *Zhang et al.* [1998] as follows:

[20] (1) Salt Fingering Regime

$$K_S = \frac{R^*}{1 + \left(\frac{R_\rho}{R_c}\right)^n)} + K^\infty \quad (7)$$

$$K_T = \frac{0.7 R^*}{R_\rho\left(1 + \left(\frac{R_\rho}{R_c}\right)^n\right)} + K^\infty, \quad (8)$$

using $n = 6$, background diffusivity $K^\infty = 5 \times 10^{-6}$ m^2 s^{-1}, $R^* = 10 \times 10^{-4}$ m^2 s^{-1}, and a critical density ratio $R_c = 1.7$.

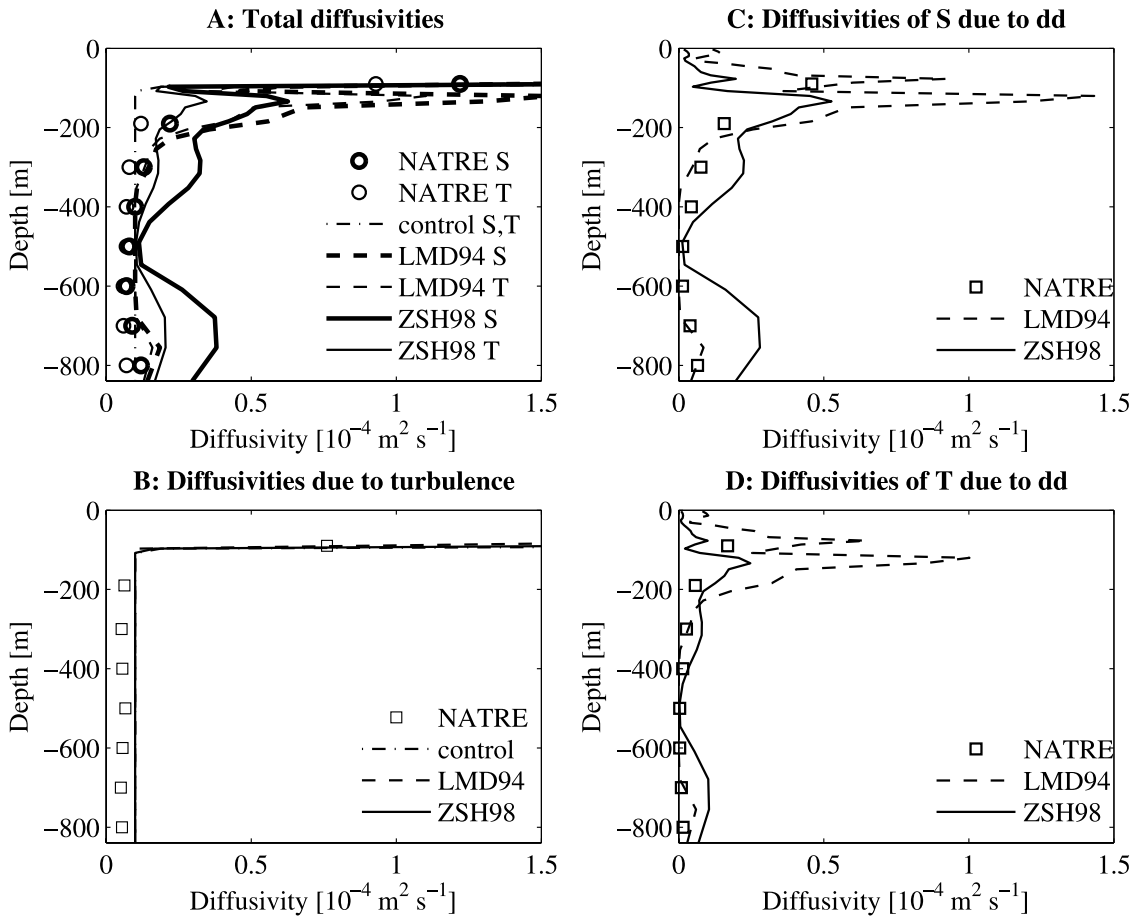

Figure 2. Diffusivities at the NATRE site and the respective contributions of normal turbulence and double diffusion. (A) Total diffusivities. (B) Diffusivities due to turbulence. (C) Diffusivities of salinity due to double diffusion. (D) Diffusivities of temperature due to double diffusion. NATRE denotes the diffusivities as determined at NATRE, LMD94 and ZSH98 are the parameterizations as described above.

[21] (2) Diffusive Layering Regime

[22] Double-diffusive mixing in the diffusive layering regime is parameterized after *Kelley* [1990] as:

$$K_T = CRa^{1/3}k_t + K^{\infty} \tag{9}$$

$$K_S = R_F R_\rho (K_T - K^{\infty}) + K^{\infty}, \tag{10}$$

with the molecular diffusivity of temperature k_t = 1.4 × 10^{-7} m^2 s^{-1} and

$$C = 0.0032 \times \exp\left(4.8R_\rho^{0.72}\right) \tag{11}$$

$$Ra = 0.25 \times 10^9 R_\rho{}^{-1.1} \tag{12}$$

$$R_F = \frac{\frac{1}{R_\rho} + 1.4\left(\frac{1}{R_\rho} - 1\right)^{3/2}}{1 + 14\left(\frac{1}{R_\rho} - 1\right)^{3/2}}. \tag{13}$$

In this study, the constant K^{∞} is replaced with the value calculated locally from the superposition of internal wave activity, static instability and local shear instability (described above).

3. Model Validation at the NATRE Site

[23] During the North Atlantic Tracer Release Experiment (NATRE) in 1992, microstructure measurements were taken in an area moderately favorable for salt fingering (approximately 26–31°W, 24–28°N [*St. Laurent and Schmitt*, 1999]). It was found that mixing by "ordinary" turbulence was sufficiently strong to prevent the formation of thermohaline staircases. However optical shadowgraph profiles showed evidence of salt fingers. Considering density ratio and Richardson number, *St. Laurent and Schmitt* [1999] computed the respective diffusivities of temperature and salt for this moderately salt-finger favorable regime. These were split up into one part due to "normal" turbulence and a second part due to salt-finger-induced mixing, according to

$$K_\theta = P^{(t)}K_0^{(t)} + P^{(f)}K_\theta^{(f)} \tag{14}$$

$$K_s = P^{(t)}K_0^{(t)} + P^{(f)}K_s^{(f)} \tag{15}$$

with weighting factors $P^{(t)}$ and $P^{(f)}$ for the relative influence of normal mixing and of salt fingering, $P^{(t)} + P^{(f)} = 1$. $K_0^{(t)}$ is

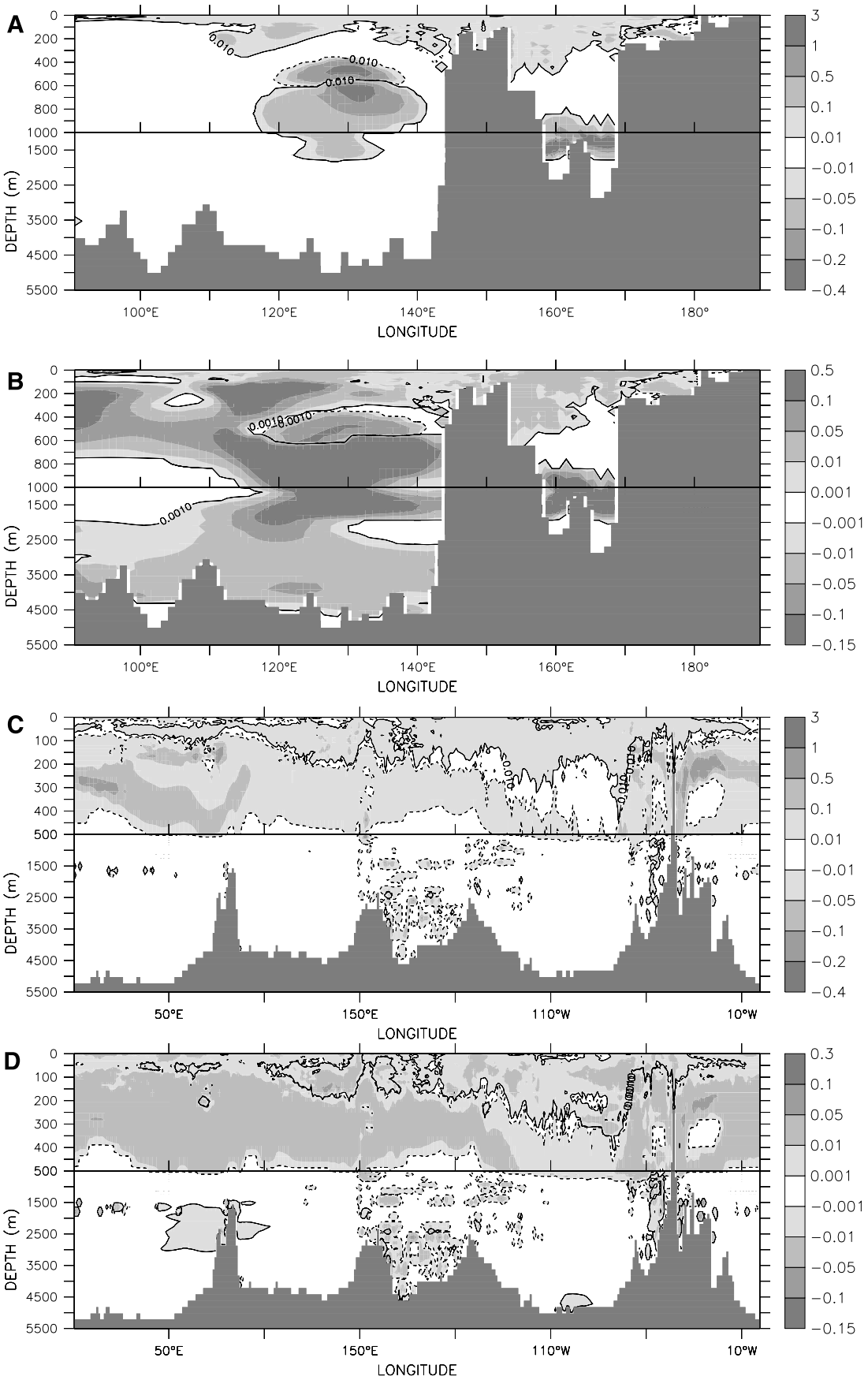
A
B
C
D
DEPTH (m)
LONGITUDE
100°E
120°E
140°E
160°E
180°
50°E
150°E
110°W
10°W
0.010
0.0010
3
1
0.5
0.1
0.01
−0.01
−0.05
−0.1
−0.2
−0.4
0.05
0.001
−0.001
−0.15
0.3

Figure 3

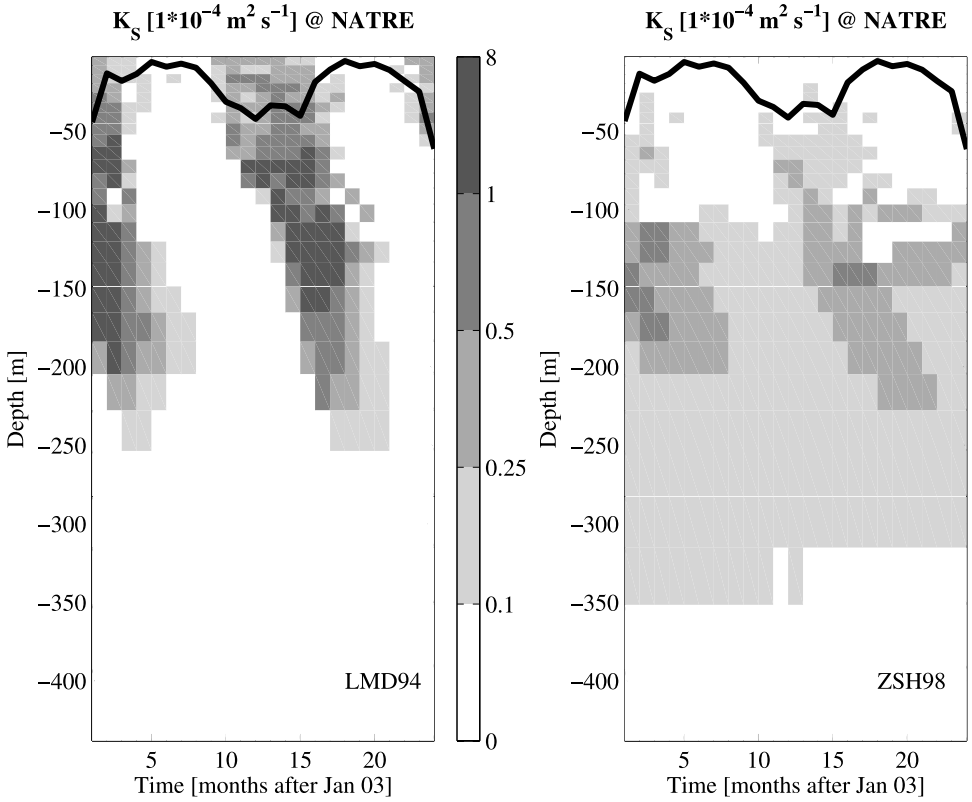

Figure 4. Annual cycle of diffusivities [10^{-4} m^2 s^{-1}] against depth [m] at the NATRE site. Red line indicates the monthly mean mixed layer depth as given by KPP.

the diffusivity estimated by assuming that the observed microstructure is caused entirely by normal mixing, $K_\theta^{(f)}$ and $K_s^{(f)}$ are the diffusivities for temperature and salinity, respectively, estimated by assuming that the microstructure is caused entirely by double diffusion. Since the model simply adds 'normal' and double-diffusive mixing coefficients, we accordingly compare the effective observed $P^{(t)}K_0^{(t)}$ with the model's normal diffusivity, and the observed $P^{(f)}K_{\theta/s}^{(f)}$ with the model's double diffusive mixing coefficients (see Figure 1, lower panel, for $P^{(f)}K_{\theta/s}^{(f)}$ as a function of the density ratio). While observations were taken in April 1992, we chose to take model results of April 2004 for this comparison, as the model was started only in 1989 from a spun-up state of a model integration without double diffusion, and we wanted to give the model fields as much time as possible to adjust to the new mixing parameterization. However comparison with other model years yielded similar results (not shown).

[24] As shown by Figure 2, the model runs all overestimate the total diffusivities, more so for the diffusivity of salinity than for the diffusivity of temperature. This already happens for the control run which, in depths greater than the mixed layer depths (in this case approximately 100 m), only uses the background value of 0.1×10^{-4} m^2 s^{-1} (see Figure 2b). Consequently, the double-diffusive runs with additional diffusivities due to double diffusion overestimate the diffusivities obtained at the NATRE experiment even more (see Figure 2a).

[25] Still, the general shape of the diffusivity profile is reproduced by the model: all three runs show enhanced mixing in the mixed layer, and the double-diffusive runs show increasing diffusivities below a minimum at about 500 m. Model run LMD94 has the upper peak in diffusivities because of the double diffusion for salinity and temperature too deep in the water column, and it overestimates diffusivities below 600 m and underestimates in between. Run ZSH98 fits observed diffusivities well in the lower part and underestimates the upper peak (see Figures 2c and 2d).

[26] Differences between the modeled and the measured diffusivities are caused both by an imperfect parameterization of (double-diffusive) mixing as well as by difficulties of the model to reproduce the temperature and salinity stratification.

[27] Applying the parameterizations LMD94 and ZSH98 to the density ratios measured at NATRE (instead of the density ratios simulated by the model) yield root-mean-square deviations from the observational estimates of the double-diffusive parts of the diffusivities of 0.5×10^{-4} m^2 s^{-1} (K_S LMD94), 0.2×10^{-4} m^2 s^{-1} (K_S ZSH98), 0.4×10^{-4} m^2 s^{-1} (K_T LMD94), and 0.1×10^{-4} m^2 s^{-1} (K_T ZSH98), respectively.

Figure 3. Differences between the diffusivity of salt and the diffusivity of temperature in cm^2 s^{-1} for the year 2004 for a north–south section (A and B) and a section at 60°S (C and D), both sections shown in Figure 5, Panel A, for LMD94 (A and C) and ZSH98 (B and D). Contours are drawn at 0.01 cm^2 s^{-1} (LMD94, solid), −0.01 cm^2 s^{-1} (LMD94, dashed), 0.001 cm^2 s^{-1} (ZSH98, solid), −0.001 cm^2 s^{-1} (ZSH98, dashed).

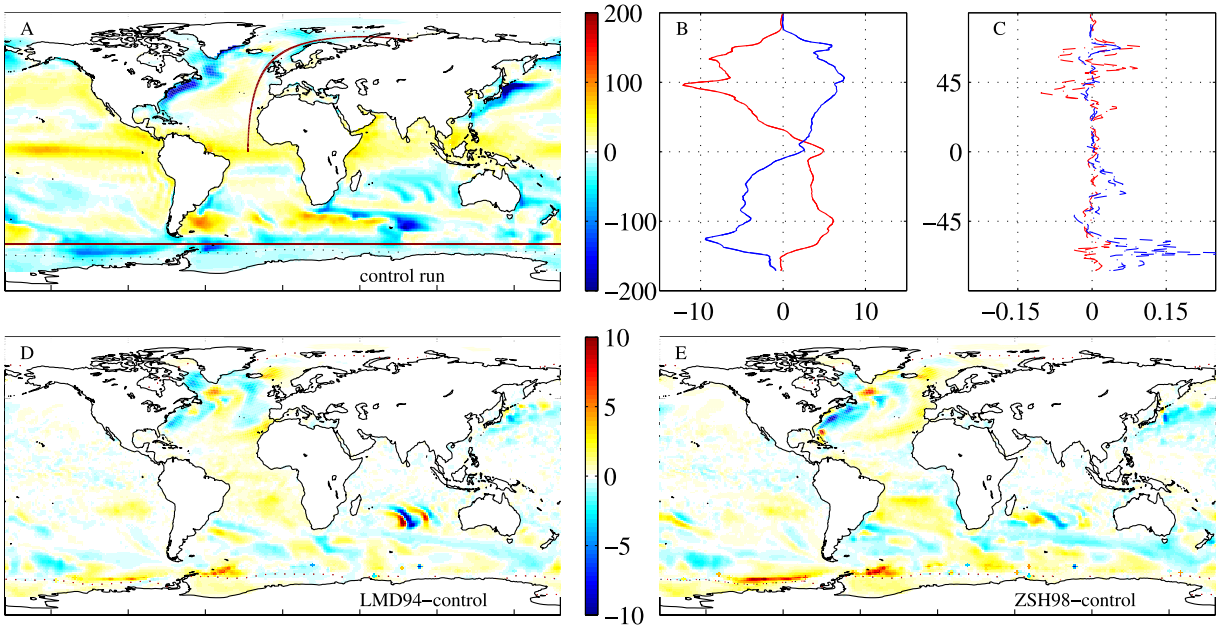

Figure 5. Simulated annual mean air-to-sea heat flux and contour of 90% sea-ice coverage (dotted line) of the control run (A, drawn in red are the sections which are shown in Figure 3). Zonal mean heat flux for January to March (red) and July to August (blue) for the control run (B). Difference of the zonal mean heat flux for January to March (red) and July to August (blue) for control-LMD94 (dashed line) and control-ZSH98 (dashed-dotted line) (C). Difference between the double-diffusive runs and the control run (LMD94-control: D, ZSH98-control: E) in heat fluxes and contour of 90% ice coverage in the control run (black dotted line) and in the double-diffusive run (red dotted line). All plots in [W m^{-2}].

This suggests a slight advantage of the ZSH98 parameterization. The difference between the total diffusivities of T and S compared as above are 0.1 $\times$ 10^{-4} m^2 s^{-1} for both parameterizations (computed all for the eight measurements in the depth range 90 m to 800 m). In comparison with NATRE data, ZSH98 does a better job in reproducing the diffusivity profiles (see Figure 2).

4. Results and Discussion

4.1. Physics

[28] In this section, changes between the double-diffusive runs and the control run are investigated with focus on physical upper ocean quantities that are potentially relevant for climate models. The regions in which double-diffusive mixing occurs in the model match those derived from observations described above: The model correctly reproduces salt fingering below, and the diffusive layering above, the Mediterranean outflow (see Figure 3). However, especially for the salt fingering regime, the extent of regions in which double-diffusive mixing is active differs between the runs—LMD94 cuts off at a lower density ratio than ZSH98, hence ZSH98 tends to display double diffusion at larger regions.

[29] In the pycnocline, salt fingering is generally strongest in subtropical regions, and diffusive layering is strongest in seasonally ice covered areas, again in agreement with observations.

[30] In the upper ocean, the spatial patterns of the different regimes show some annual cycle, particularly close to the seasonally varying sea ice edge which tends to separate diffusive layering and salt fingering regimes. The regions with most active near-surface salt fingering also move with the seasons from one winter hemisphere to the other. At a given station located in the subtropical salt-fingering regime, double-diffusive mixing usually sets in at the bottom of the mixed layer in autumn when the winter mixed layer is about to reach its maximum depth. Over the next few months the region over which double diffusion is active spreads both upward and downward until a maximum intensity and a maximum vertical extent of double-diffusive mixing are reached. The depth of maximum salt fingering in spring is typically a couple of tens to a hundred meters deeper than the depth at which double diffusion set in autumn. The annual cycle of diffusivities at a typical subtropical site (the NATRE region) is shown in Figure 4.

[31] As a result of the annual cycle in salt fingering, the impact of double diffusion on air–sea heat fluxes is largest at the end of winter. Although the intensity of double diffusive mixing usually reaches its maximum only later in the year, this maximum occurs well below the surface mixed layer and thus does not have immediate contact with the atmosphere. Consequently, the impact of double diffusion on surface fluxes (not only of heat but also of gases, see below) is generally bigger in the respective winter hemisphere than in the summer hemisphere (Figure 5). Typical values for the zonally and seasonally averaged changes in the simulated surface heat flux because of the double diffusion are 0.1 W m^{-2} in the winter hemisphere and an order of magnitude less in the summer hemisphere.

[32] Local effects of double diffusion on surface heat fluxes through changes in SST are in the range of $\pm$30 W m^{-2}. The maximum values are reached only at

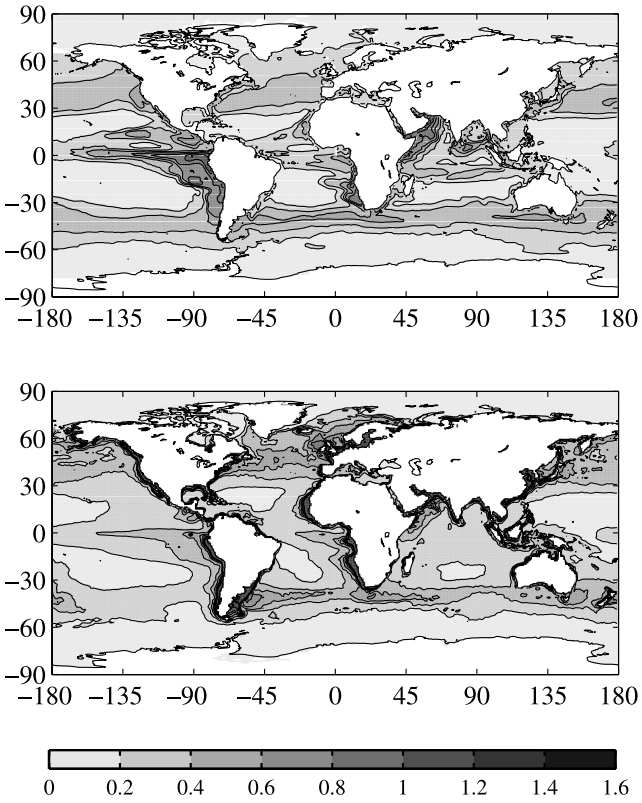

Figure 6. Comparison of annual mean integrated production [g C m^{-2} d^{-1}] as modeled in the reference run (top) and annual mean integrated production after *Behrenfeld and Falkowski* [1997] (bottom).

a few isolated grid points in the Bering Strait and at the ice edge near Antarctica, and result from small changes in the ice coverage mentioned above. As shown in Figure 5, systematic larger-scale impacts occur in the subtropical and the subpolar regions prone to near-surface salt-finger activity: As salt fingers transport both heat and salt downward, the sea surface is cooled and the heat loss to the atmosphere is reduced, enhancing the large-scale net heat flux into the ocean by typically 0.05 to 0.1 W m^{-2}. Somewhat larger changes are found in the Gulf Stream and Kuroshio regions, with magnitude ± 10 W m^{-2} for run ZSH98 and ±5 W m^{-2} for run LMD94 (± depending on the side of the front). In these areas of strong lateral gradients in SST, even small changes in circulation patterns can have a large local effect on air–sea heat fluxes. Given that typical surface heat fluxes in these western boundary-current regions can reach several hundred W m^{-2}, the modifications induced by double diffusion are relatively small.

[33] The locally enhanced impacts of double-diffusion on air–sea heat exchange in the southern part of the Indian Ocean result from a small phase shift in a slowly moving wave, probably related to an interaction of basin scale atmospheric forcing with eastern boundary processes (*Birol and Morrow* [2001]).

[34] Near-surface double diffusion also affects sea surface salinity, although this effect may be underestimated in the model because of the sea surface salinity relaxation mentioned above. Changes between the runs are mainly a freshening of the sea surface for the double-diffusive runs, resulting from the net downward flux of salt by double diffusion. Via the surface salinity relaxation condition, this leads to a decreased freshwater flux into the ocean. Run LMD94 receives about 21 mm $year^{-1}$ less freshwater in the annual mean 2004 than the control run. For ZSH98 the decrease is approximately 42 mm $year^{-1}$. For reference, the control run receives 611 mm $year^{-1}$ freshwater, thereof 225.3 mm $year^{-1}$ via the sea surface salinity (SSS) relaxation.

[35] Changes in the modeled sea-ice fields are potentially important because they may have a big impact on the modeled surface albedo and surface heat fluxes. Our experiments show that changes in ice fields due to double diffusion are very small, the ice cover is enhanced compared to the control run (average increase over the simulated year 2004: ZSH98 southern hemisphere 0.8%, northern hemisphere 0.1%; LMD94 southern hemisphere 0.3%, northern hemisphere 0.1%).

[36] For completeness we note that in our model runs, the inclusion of double diffusion has little impact on the depth of the surface mixed layers, with changes always far smaller than the thickness of a grid box. Furthermore, double diffusion has no significant impact on the mean circulation, including the meridional overturning circulation, within the 16 years we ran our models for. For a complete assessment of large-scale circulation changes much longer runs would be required.

4.2. Primary Production and Nutrient Supply

[37] In general, relative changes due to double diffusion are much larger for the simulated biogeochemical properties compared to the physical properties discussed above. Simulated primary production is enhanced by double-diffusive mixing in most regions. The strongest increase in regional primary production by more than 120% for ZSH98 and 80% for LMD94 can be found in the subtropical Atlantic, where double-diffusive mixing acts strongly at the depth of the nutricline (Figure 7).

[38] Nitrate supply into the upper 127 m occurs mainly around 40°N and 40°S and in upwelling areas. In low-latitude and Southern-Ocean upwelling areas, this happens partly via vertical advection whereas the largest part of the supply in mid-latitudes is due to convection in autumn and winter. The largest changes between the double-diffusive runs and the control run occur in the Atlantic at 20°N and between 10 and 30°S, and at 20°S off South America in the Pacific. In these regions, double diffusion alters the stratification such that convection becomes slightly deeper than in the control run.

[39] Surface nitrate concentrations of the normal run overall compare well with nitrate documented in World Ocean Atlas by *Levitus* [1994]. However the model tends to underestimate concentrations in the subtropics and tropics. These are the regions where double diffusion brings up nutrients into the eutrophic zone however not enough to match the world ocean atlas (at least not at the surface). The model overestimates nitrate concentrations in the Arctic, but this feature is over-emphasized by the map projection.

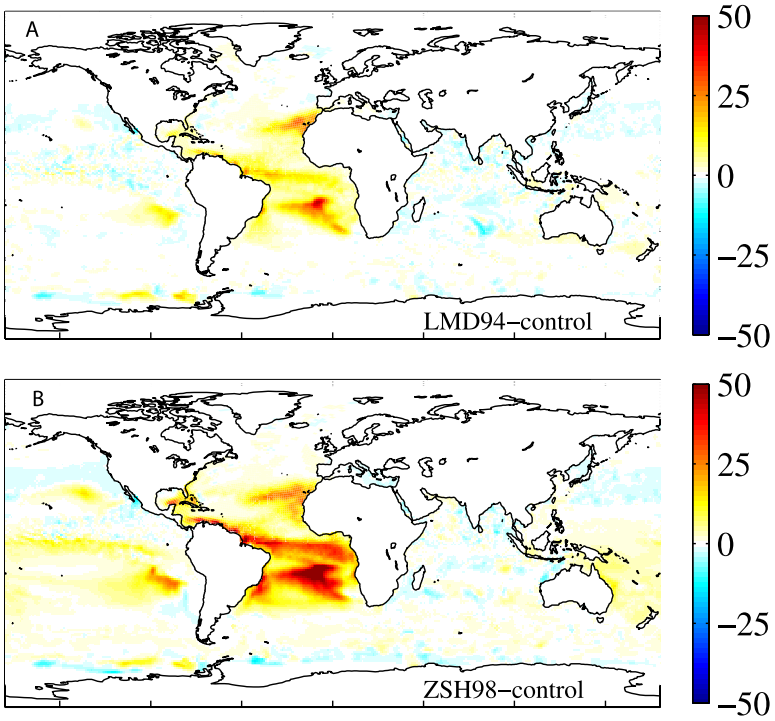

Figure 7. Difference in vertically integrated primary production simulated for the year 2004 between the double-diffusive runs and the control run (LMD94-control: A, ZSH98-control: B). All plots in [g C m^{-2} a^{-1}].

[40] On the global average, nitrate supply into the upper 127 m increases by 0.001 mol N m^{-2} $year^{-1}$ on switching from the control run to experiment LMD94, and 0.006 mol N m^{-2} $year^{-1}$ when switching from control to experiment ZSH98. In both cases, most of this additional supply occurs in mid latitudes. These results are consistent with those reported by *Oschlies et al.* [2003], who found typical fluxes of 0.03 mol N m^{-2} $year^{-1}$ due to salt fingering instabilities in the subtropical North Atlantic. For the same region, our experiments yield 0.02 mol N m^{-2} $year^{-1}$ more uptake for MD94 and 0.04 mol N m^{-2} $year^{-1}$ for ZSH98.

4.3. Surface Fluxes of CO_2 and O_2

[41] After less than two decades of spin up, the model's oceanic carbon inventory is not in complete equilibrium, and the ocean is outgassing CO_2 to the atmosphere (kept at constant, pre-industrial pCO_2 of 278 ppm). The annual CO_2 sea-to-air flux for the control run is 8.3 g C m^{-2} $year^{-1}$, whereas for the double-diffusive runs outgassing is reduced to 7.9 g C m^{-2} $year^{-1}$. Initially, we suspected that the additional CO_2 uptake in the double diffusive run was occurring in the subtropics, where primary production is enhanced by double-diffusive mixing and where surface temperatures are reduced by the action of double diffusion. Thus both enhanced biotic uptake of CO_2 and the enhanced gas solubility in colder surface waters act to increase oceanic CO_2 uptake. However, as shown in Figure 9, the double diffusive runs instead show enhanced outgassing in the subtropics. To understand this unexpected behavior, we investigate the changes in oceanic pCO_2 as a function of temperature, salinity, the DIC concentration and alkalinity. Total pCO_2 changes are partitioned into contributions from changes in surface salinity, temperature and DIC according to

$$\Delta pCO_2 = \frac{\delta pCO_2}{\delta S}\Delta S + \frac{\delta pCO_2}{\delta T}\Delta T + \frac{\delta pCO_2}{\delta DIC}\Delta DIC + o\left(\Delta^2\right). \tag{16}$$

where ΔpCO_2, ΔS, ΔT and ΔDIC represent the difference of pCO_2, surface salinity, surface temperature, and surface DIC between double diffusive run and control run, respectively, and $o(\Delta^2)$ represents terms of second and higher orders in the perturbed quantities. The partial derivatives are taken as $\frac{\delta pCO_2}{\delta T} \approx 10$ ppm K^{-1}, $\frac{\delta pCO_2}{\delta DIC} \approx 1$ ppm $mmol^{-1}$ m^3 and $\frac{\delta pCO_2}{\delta S} \approx -60$ ppm psu^{-1} (e.g., *Eden and Oschlies* [2006]). The differences in surface temperature between the double diffusive runs and the control run vary regionally. In the zonal mean, the strongest feature are a cooling at about 60°N/S, a cooling around 20°N/S and a warming at about 45°N/S. However these changes in surface temperature have only a relatively small effect on changes in pCO_2. As shown in Figure 9, the changes in pCO_2 because of the changes in salinity and DIC are much larger, and rather than oscillating around zero they are distinctly positive for salinity and distinctly negative for DIC. Sea surface salinity is lower almost everywhere in the double diffusive runs than in the control run. A lower salinity, in the model, corresponds to lower alkalinity and hence higher pCO_2.

[42] In our model, the negative ΔS is mirrored in the P-E relaxation: Restoring SSS to Levitus leads to artificial changes in P-E in response to double-diffusive mixing,

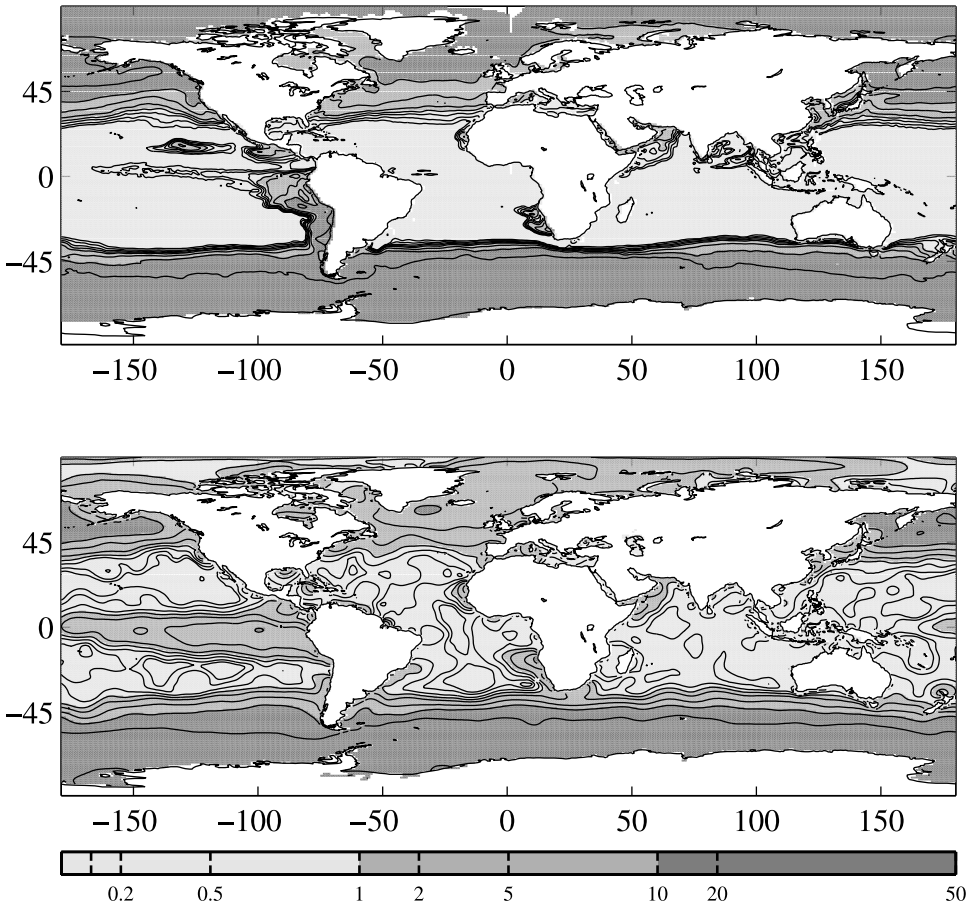

Figure 8. Comparison of nitrate [mmol N m^{-3}] in the control run (top) and in World Ocean Atlas by *Levitus* [1994] (bottom).

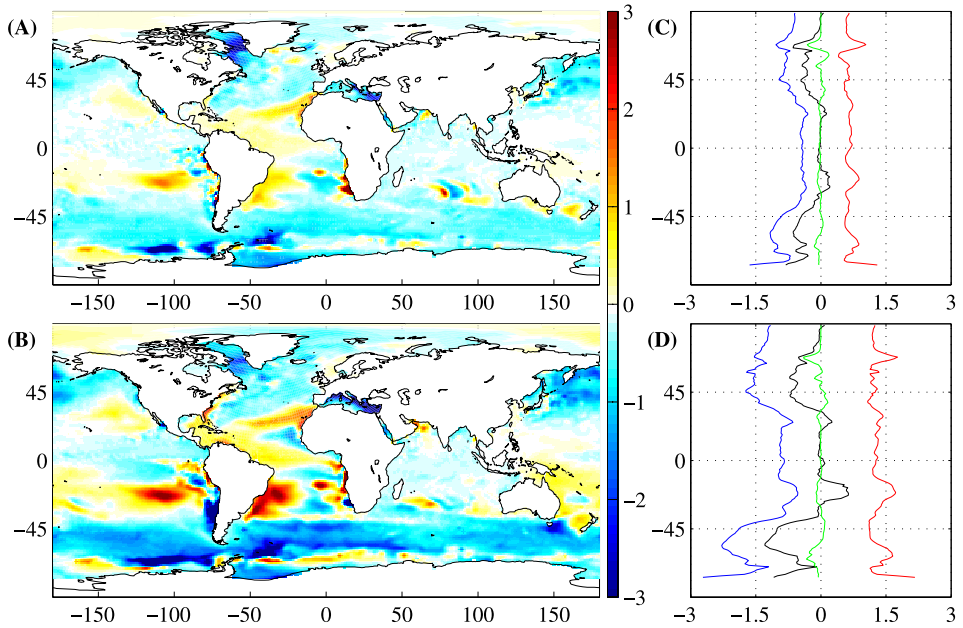

Figure 9. Differences in simulated surface pCO_2 between double-diffusive run and control run (Plot a: LMD94-control. Plot b: ZSH98-control) and zonal mean of the partitions of the influence of T, S and DIC to the total pCO_2 difference calculated from $\Delta pCO_2 = \frac{\delta pCO_2}{\delta S}\Delta S + \frac{\delta pCO_2}{\delta T}\Delta T + \frac{\delta pCO_2}{\delta DIC}\Delta DIC + o(\Delta^2)$ after *Eden and Oschlies* [2006]. Black line: ΔpCO_2, green line: $\frac{\delta pCO_2}{\delta T}\Delta T$, red line: $\frac{\delta pCO_2}{\delta S}\Delta S$ and blue line: $\frac{\delta pCO_2}{\delta DIC}\Delta DIC$ for LMD94-control (plot c) and ZSH98-control (plot d).

whereas such a feedback does not exist in reality. Less freshwater (equivalent to more salt) is added to the double diffusive runs compared to the control run. Thereby restoring SSSs weakens differences in SSS (which translate to differences in alkalinity) between the runs. This challenges the ΔpCO_2 derived in this study. If it was not for the relaxation, ΔS would be bigger than it is now, therefore the influence of the difference in salinity (and alkalinity) might be even larger compared to the other two terms, and the model ocean might release even more CO_2 to the atmosphere once double-diffusive mixing is accounted for. Additionally restoring prevents the salinity stratification from erosion by double-diffusive fluxes and thereby tampers with the double-diffusive potential of the stratification. The SSS relaxation influences alkalinity even though in this model alkalinity is a prognostic tracer, only linked to salinity through the P-E fluxes, because the relaxation is achieved through surface freshwater fluxes.

[43] ΔDIC is negative almost everywhere, too. Because pCO_2 decreases with decreasing DIC, the changes in surface DIC and surface salinity tend to oppose each other. Compared to the effects of salinity changes, changes in the photosynthetical drawdown of DIC are small in the subtropics. On the other hand, the subpolar and polar decreases of pCO_2 in the double-diffusive runs are mostly due to the changes in surface DIC. As in the subtropics, salinity changes act to counteract the ΔDIC-related pCO_2 reduction but, in contrast to the subtropics, has a smaller magnitude (see Figure 9).

[44] Annual O_2 air–sea fluxes of our model runs compare well with those simulated by *Bopp et al.* [2002]. Oceanic O_2 uptake is reduced almost everywhere in the double diffusive runs compared to the control run (approximately 0.2 mol m^{-2} $year^{-1}$) despite lower SSTs which should lead to more O_2 being taken up. This can be explained by the higher biological productivity (more photosynthesis, hence more production of O_2) In contrast to CO_2, oxygen does not react with seawater, but instead dissolves in it. As such, it is unaffected by changes in surface alkalinity and carbonate chemistry, although there is a small salinity effect on oxygen saturation.

5. Summary

[45] Two different parameterizations of double-diffusive mixing, ZDH98 and LMD94, have been applied to a global ocean ecosystem-circulation model. Both parameterizations formulate double-diffusive mixing in terms of the density ratio, although mixing intensities and the ranges of relevant density ratios differ considerably (Figure 1). When applied to density ratios measured at NATRE, modeled diffusivities are closer to observational estimates for ZSH98 than for LMD94. This suggests that ZSH98 is a more realistic description of double diffusive mixing than is LMD94.

[46] A recent update of the LMD94 parameterization [*Danabasoglu et al.*, 2006], which uses a higher cut-off density ratio and a lower maximum diffusivity, produces diffusivities closer to those of ZSH98. We did not include this update in our intercomparison directed at the sensitivity of model results to different parameterizations because the updated parameterization appears to lie between LMD94 and ZSH98.

[47] Differences between the double-diffusive runs and the control run are almost always larger for ZSH98 than for LMD94. This happens because ZSH98 applies the parameterization of double diffusion to a larger range of density ratios than LMD94 does and hence simulates non-zero salt-finger-related diffusivities over larger parts of the ocean (Figure 3). The fact that diffusivities of LMD94 are up to a factor 10 higher than ZSH98 for density ratios close to 1 has only limited effect in the current model. This might be related to the still relatively coarse vertical grid that does not resolve sharp vertical property gradients and may hence influence how often situations with a density ratio close to 1 occur.

[48] The results of our study suggest only limited effect of double diffusion on physical upper ocean properties, though our decadal-scale simulations do not enable us to rule out longer-term changes in the ocean circulation as have been reported for some models [*Merryfield et al.*, 1999; *Zhang and Schmitt*, 2000]. In our model, the changes in heat fluxes between the double-diffusive runs and the control run turn out to be more than an order of magnitude smaller than the fluxes associated with the current anthropogenic greenhouse effect which are thought to be of the order of 2.5 W m^{-2} [*Soon et al.*, 2000]. The most dramatic effects of including double diffusive mixing were found for the marine biology and biogeochemistry. Primary production shows regional enhancements by some 100% over large areas of the oligotrophic subtropical gyres. Global enhancement is much smaller, about 1% for LMD94 and 3% for ZSH98, because the large relative enhancement takes place mostly in low-productivity regions. Simulated CO_2 uptake of the ocean is enhanced by about 0.14 Gt C $year^{-1}$ in the double diffusive runs. This is about 7% of the anthropogenic CO_2 signal (which is approximately 2 Gt C $year^{-1}$ according to *Sarmiento and Sundquist* [1992]; *Takahashi et al.* [2002]).

[49] The climate sensitivity of double-diffusive mixing differs from that of ''ordinary'' mixing processes as, for example, mixing due to internal waves. Whereas in the case of ''ordinary'' mixing processes the intensity of mixing depends on the stability of the density stratification, double-diffusive mixing is thought to be a function of the density ratio, i.e., of the relative contributions of the vertical temperature and salinity gradients to the vertical density profile. As it is likely that global warming will lead to changes in the proportion of ''ordinary'' mixing to double-diffusive mixing [*Oschlies et al.*, 2003], estimates of future climate change will benefit from a better quantitative understanding of double-diffusive mixing.

[50] Although this modeling study cannot yield a definite conclusion about which parameterization is more realistic, the influence of double-diffusive mixing on upper ocean properties should be kept in mind (if not accounted for) in long climate-study runs. The main result of this study is that our mechanistic understanding of mixing processes, and their parameterizations in ocean circulation models, are not yet satisfactory. Implementing a small-scale and supposedly unimportant mixing process showed that tiny changes in mixing can have global impacts, particularly on the upper ocean biology which reacts in a highly non-linear way to changes in nutrient supply. A better understanding of mixing processes (including, but not limited to, double diffusion) is important in order for models to accurately

simulate real-world behavior—including that caused by anthropogenically-driven climate change.

Appendix A: Parameterizations of Double Diffusive Mixing

A1. Parameterization LMD94 of Double Diffusive Mixing

A1.1. Double Diffusive Mixing in the Salt Fingering Regime

[51] Double-diffusive mixing in the salt fingering regime is parameterized following an analysis of limited observational data by *Schmitt* [1981, 1988]. Mixing is found to be at background levels (about 10^{-5} m^2 s^{-1}) for $R_\rho > 1.9$, then rapidly increasing near $R_\rho = 1.7$ and to be large for $R_\rho < 1.5$ (about 10^{-3} m^2 s^{-1}). Mixing of temperature is found to behave in a similar fashion, but to be less intense at the same density ratio. A curve fit leads to the following equations

$$K_s = K_f \left[1 - \left(\frac{R_\rho - 1}{R_\rho^0 - 1}\right)^2\right]^p \quad \text{for } 1 < R_\rho < R_\rho^0 \tag{A1}$$

$$K_s = 0.0 \text{ for } R_\rho \geq R_\rho^0 \tag{A2}$$

$$K_\theta = 0.7 K_s \tag{A3}$$

where K_s is the diffusivity of salinity due to double-diffusive mixing, K_θ is the diffusivity of potential temperature due to double-diffusive mixing, $K_f = 10 \times 10^{-4}$ m^2 s^{-1} is the maximum of the diffusivity due to salt fingering, $R_\rho^0 = 1.9$ is the critical density ratio above which mixing due to double diffusion is assumed to be not effective any more, and $p = 3$. The diffusivity of salt is computed indirectly by applying a laboratory flux law to observed salinity steps in staircase regions and then dividing by the mean salinity gradient. However laboratory flux laws are not necessarily valid in the open ocean because of, for example, background internal wave fields which are present in the ocean but difficult to reproduce in the laboratory [*Gargett*, 1989; *Kelley et al.*, 2003].

A1.2. Double-Diffusive Mixing in the Diffusive Layering Regime

[52] Double-diffusive mixing of temperature in the diffusive layering regime is parameterized after *Large et al.* [1994] as

$$K_\theta = 0.909^* \exp\left(4.6^* \exp\left[-0.54\left(R_\rho^{-1} - 1\right)\right]\right)\nu \tag{A4}$$

with the molecular viscosity $\nu = 1.5 \times 10^{-6}$ m^2 s^{-1}. The diffusivity of salt is

$$K_s = K_\theta\left(1.85 - 0.85 R_\rho^{-1}\right) R_\rho \text{ for } 0.5 \leq R_\rho < 1 \tag{A5}$$

$$K_s = K_\theta 0.15 R_\rho \text{ for } R_\rho < 0.5 \tag{A6}$$

This parameterization goes back to tank experiments and theoretical considerations as well as dimensional arguments [*Turner*, 1965; *Fedorov*, 1988; *Marmorino and Caldwell*, 1978; *Huppert*, 1971]. According to *Large et al.* [1994], the sequence of subroutine calls in the model code was such that double diffusion was called before the mixed layer mixing was calculated. The order of calls was changed here, such that double diffusion is now called at the end. Therefore the "normal" mixing can be clearly distinguished from the additional mixing due to double diffusion.

A2. Parameterization ZSH98 of Double-Diffusive Mixing

A2.1. Double-Diffusive Mixing in the Salt Fingering Regime

[53] The effective diffusivities for temperature and salinity, R_T and R_S, are parameterized by *Zhang et al.* [1998], as:

$$K_S = \frac{R^*}{1 + \left(\frac{R_\rho}{R_c}\right)^n} + K^\infty \tag{A7}$$

$$K_T = \frac{0.7R^*}{R_\rho\left(1 + \left(\frac{R_\rho}{R_c}\right)^n\right)} + K^\infty \tag{A8}$$

This parameterization is quoted from *Schmitt* [1981] who used the slightly different relation $K_T = \frac{0.7}{R_\rho} R_K$, with $R^* = 10 \times 10^{-4}$ m^2 s^{-1}. In the present study we will employ the *Zhang et al.* [1998] parameterization, using different values than originally proposed by *Schmitt* [1981], "reflecting improved understanding of fluxes in the thermohaline staircases observed in the C-SALT program" [*Schmitt*, 1988]: $n = 6$, background diffusivity $K^\infty = 5 \times 10^{-6}$ m^2 s^{-1} and a critical density ratio $R_c = 1.7$. The intensity of salt-finger convection is described as a strong function of R_ρ. This formulation of the diffusivities was chosen because of the simple specification of a cut-off R_ρ and the ability to make the cut-off as sharp as desired (by increasing n). This pragmatic parameterization has "no theoretical basis whatsoever" [*Schmitt*, 1981], it only allows to reproduce the apparent dependence of the diffusivities on R_ρ suggested by the application of laboratory flux laws to oceanic fine structure data.

A2.2. Double-Diffusive Mixing in the Diffusive Layering Regime

[54] Double-diffusive mixing in the diffusive layering regime is parameterized after *Kelley* [1990]. K_T and K_S are described as:

$$K_T = CRa^{1/3} k_t \tag{A9}$$

$$K_S = R_F R_\rho K_T \tag{A10}$$

with the molecular diffusivity of temperature $k_t = 1.4 \times 10^{-7}$ m^2 s^{-1} and

$$C = 0.0032 \times \exp\left(4.8 R_\rho^{0.72}\right) \tag{A11}$$

$$Ra = 0.25 \times 10^9 {R_\rho}^{-1.1} \tag{A12}$$

$$R_F = \frac{\frac{1}{R_\rho} + 1.4\left(\frac{1}{R_\rho} - 1\right)^{3/2}}{1 + 14\left(\frac{1}{R_\rho} - 1\right)^{3/2}}. \tag{A13}$$

This is the same as used by *Kelley* [1984], apart from new formulations of C and R_F which were fitted to the whole collection of laboratory measurements available at that time. *Zhang et al.* [1998] included diffusivities unrelated to

double-diffusive mixing, K^{∞} to the formulation above, modifying equations (A9) and (A10) to

$$K_T = CRa^{1/3}k_t + K^{\infty} \tag{A14}$$

$$K_S = R_F R_\rho (K_T - K^{\infty}) + K^{\infty}, \tag{A15}$$

but as they did not use a turbulence model, they approximated the diffusivity caused by processes not related to double diffusion as $K^{\infty} = 0.3 \times 10^{-4}$ m^2 s^{-1}. In this study, the constant K^{∞} is replaced with the value calculated from the superposition of internal wave activity, static instability and local shear instability (described above). *Zhang et al.* [1998] apply double-diffusive mixing only where the magnitude of the vertical temperature gradient $T_Z = \frac{\delta T}{\delta Z}$ is larger than a critical value $T_{Z,C} = 25 \times 10^{-4\circ}$ C m^{-1} to restrict double-diffusive mixing to the thermocline. This restriction is not applied in the present study.

[55] **Acknowledgments.** We are grateful to Bablu Sinha for assistance with nutrient transport diagnostics and for operational assistance with OCCAM. We would like to thank two anonymous reviewers for their constructive comments that helped to improve the manuscript. Also we would like to thank the German National Academic Foundation for funding parts of this study, and the National Oceanography Centre, Southampton, for hosting MSG and for computer resources. Financial support by the Deutsche Forschungsgemeinschaft through SFB 460 is acknowledged.

References

Aksenov, Y. (2002), The sea ice-ocean global coupled ARCICE project report part 1: Description of dynamical-thermodynamical sea ice model, *SOC Research & Consultancy Report 103*.

Behrenfeld, M. J., and P. G. Falkowski (1997), Photosynthetic rates derived from satellite-based chlorophyll concentration, *Limnol. Oceanogr.*, *42*, 1–20.

Birol, F., and R. Morrow (2001), Source of the baroclinic waves in the southeast Indian Ocean, *J. Geophys. Res.*, *106*, 9145–9160.

Bopp, L., C. L. Quéré, M. Heimann, A. C. Manning, and P. Monfray (2002), Climate-induced oceanic oxygen fluxes: Implications for the contemporary carbon budget, *Global Biogeochem. Cycles*, *16*(2), 1022, doi:10.1029/2001GB001445.

Conkright, M. E., R. A. Locarnini, H. E. Garcia, T. D. O'Brien, T. P. Boyer, C. Stephens, and J. I. Antonov (2002), World ocean atlas 2001: Objective analyses, data statistics, and figures, CD-rom documentation, National Oceanographic Data Center, Silver Spring, MD, USA, *Internal Report 17*, p. 17.

Coward, A. C., and B. A. de Cuevas (2005), The OCCAM 66 level model: Physics, initial conditions and external forcing, *Southampton Oceanography Centre Internal Report*, *99*, 58 pp.

Danabasoglu, G., W. G. Large, J. J. Tribbia, P. R. Gent, B. P. Briegleb, and J. C. McWilliams (2006), Diurnal coupling in the tropical oceans of CCSM3, *J. Clim.*, Special Issue.

Dietze, H., A. Oschlies, and P. Kähler (2004), Internal-wave-induced and double-diffusive nutrient fluxes to the nutrient-consuming surface layer in the oligotrophic subtropical north Atlantic, *Ocean Dyn.*, *54*, 1–7.

Eden, C., and A. Oschlies (2006), Adiabatic reduction of circulation-related CO_2 air–sea flux biases in a north Atlantic carbon-cycle model, *Global Biogeochem. Cycles*, *20*, GB2008, doi:10.1029/2005GB002521.

Fedorov, K. N. (1988), Layer thickness and effective diffusivities in the "diffusive" thermohaline convection in the ocean, 471–479 pp., Elsevier Oceanography Series.

Gargett, A. E. (1989), Ocean turbulence, *Ann. Rev. Fluid Mech.*, *21*, 419–451.

Griffies, S. M., C. Böning, F. O. Bryan, E. P. Chassignet, R. Gerdes, H. Hasumi, A. Hirst, A.-M. Treguier, and D. Webb (2000), Developments in ocean climate modeling, *Ocean Modell.*, *2*, 123–192.

Hunke, E. C., and J. K. Dukowicz (1997), An elastic–viscous–plastic model for sea ice dynamics, *J. Phys. Oceanogr.*, *27*, 1849–1867.

Huppert, H. E. (1971), On the stability of a series of double-diffusive layers, *Deep-Sea Res.*, *18*, 1005–1021.

Jevons, W. S. (1857), On the cirrus form of clouds, *Philos. Mag. J. Sci.*, *14*(90), 22–35.

Johnson, G. C. (2006), Generation and initial evolution of a mode water θ-S anomaly, *J. Phys. Oceanogr.*, *36*, 739–751.

Kelley, D. E. (1984), Effective diffusivities within oceanic thermohaline staircases, *J. Geophys. Res.*, *89*(C6), 10,484–10,488.

Kelley, D. E. (1990), Fluxes through diffusive staircases: A new formulation, *J. Geophys. Res.*, *95*(C3), 3365–3371.

Kelley, D. E., H. J. S. Fernando, A. E. Gargett, J. Tanny, and E. Özsoy (2003), The diffusive regime of double-diffusive convection, *Prog. Oceanogr.*, *56*(3–4), 461–481.

Key, R. M., et al. (2004), A global ocean carbon climatology: Results from global data analysis project (glodap), *Global Biogeochem. Cycles*, *18*, GB4031, doi:10.1029/2004GB002247.

Large, W. G., J. C. McWilliams, and S. C. Doney (1994), Oceanic vertical mixing: A review and a model with a nonlocal boundary layer parameterization, *Rev. Geophys.*, *32*(4), 363–403.

Large, W. G., G. Danabasoglu, and S. C. Doney (1997), Sensitivity to surface forcing and boundary layer mixing in a global ocean model: Annual-mean climatology, *J. Phys. Oceanogr.*, *27*, 2418–2446.

Levitus, S. (1994), World Ocean Atlas, *CD-ROM Data Set Documentation*, NODC Ocean Climate Laboratory, Washington, D. C., *Informal Report No. 13*.

Marmorino, G. O., and D. R. Caldwell (1978), Heat and salt transport through a diffusive thermohaline interface, *Deep-Sea Res.*, *23*, 59–67.

Merryfield, W. J., G. Holloway, and A. E. Gargett (1999), A global ocean model with double-diffusive mixing, *J. Phys. Oceanogr.*, *29*, 1124–1142.

Najjar, R., and J. C. Orr (1999), Biotic-HOWTO, LSCE/CEA Saclay, Gif-sur-Yvette, France, *Internal OCMIP Report*, 15 pp.

Orr, J. C., R. Najjar, C. L. Sabine, and F. Joos (1999), Abiotic-HOWTO, LSCE/CEA Saclay, Gif-sur-Yvette, France, *Internal OCMIP Report*, 25 pp.

Oschlies, A. (2001), Model-derived estimates of new production: New results point towards lower values, *Deep-Sea Res.*, *48*, 2173–2197.

Oschlies, A., H. Dietze, and P. Kähler (2003), Salt-finger driven enhancement of upper ocean nutrient supply, *Geophys. Res. Lett.*, *30*(23), 2204, doi:10.1029/2003GL018552.

Rudels, B., G. Björk, R. D. Muench, and U. Schauer (1999), Double-diffusive layering in the Eurasian basin of the arctic ocean, *J. Mar. Syst.*, *21*, 3–27.

Sarmiento, J. L., and E. T. Sundquist (1992), Revised budget for the oceanic uptake of anthropogenic carbon dioxide, *Nature*, *356*, 589–593.

Schmitt, R. W. (1981), Form of the temperature–salinity relationship in the central water: Evidence for double-diffusive mixing, *J. Phys. Oceanogr.*, *11*, 1015–1026.

Schmitt, R. W. (1987), C-salt, an investigation of the thermohaline staircase in the western tropical north Atlantic, *Deep-Sea Res.*, *34*(10A), 1655–1665.

Schmitt, R. W. (1988), Mixing in a thermohaline staircase, *Elsevier Oceanography Series*, 435–452 pp.

Semtner, A. J. (1976), A model for the thermodynamic growth of sea ice in numerical investigations of climate, *J. Phys. Oceanogr.*, *6*, 379–389.

Sinha, B., and A. Yool (2006), Extension of the OCCAM 1 deg ocean general circulation model to include the biogeochemical cycles of carbon and oxygen, part I: Technical description, *National Oceanography Centre, Southampton, Research & Consultancy Report 5*, pp. 1–78.

Soon, W., S. Baliunas, K. Y. Kondratyev, S. B. Idso, and E. S. Posmentier (2000), Calculating the climatic impacts of increased CO_2: The issue of model validation, *First Eurocongress on The Solar Cycle and Terrestial Climate Tenerife, Spain, September 25–30, 2000*.

St. Laurent, L., and R. W. Schmitt (1999), The contribution of salt fingers to vertical mixing in the North Atlantic Tracer Release Experiment, *J. Phys. Oceanogr.*, *29*, 1404–1424.

Stommel, H., A. B. Arons, and D. Blanchard (1956), An oceanographic curiosity: The perpetual salt fountain, *Deep-Sea Res.*, *3*, 152–153.

Takahashi, T., et al. (2002), Global sea-air CO_2 flux based on climatological surface ocean pCO_2, and seasonal biological and temperature effects, *Deep-Sea Res. II*, *49*, 1601–1622.

Timmermans, M.-L., C. Garrett, and E. Carmack (2004), The thermohaline structure and evolution of the deep waters in the Canada Biassin Arctic Ocean, *Deep-Sea Res. I*, *50*, 1305–1321.

Turner, J. S. (1965), The coupled transport of salt and heat across a sharp density interface, *Int. J. Heat Mass Transfer*, *8*, 759–767.

Yool, A., and B. Sinha (2006), Extension of the OCCAM 1 deg ocean general circulation model to include the biogeochemical cycles of carbon and oxygen, part ii: Initial experiments, National Oceanography Centre, Southampton, *Research & Consultancy Report 6*.

You, Y. (2002), A global ocean climatological atlas of the Turner angle: implications for double-diffusion and water-mass structure, *Deep-Sea Res. I*, *49*, 2075–2093.

Zenk, W. (1970), On the temperature and salinity structure of the Mediterranean water in the northeast Atlantic, *Deep-Sea Res.*, *17*, 627–631.

Zhang, J., and R. W. Schmitt (2000), The impact of salt fingering on the thermohaline circulation under mixed boundary conditions, *J. Phys. Oceanogr.*, *30*, 1223–1231.

Zhang, J., R. W. Schmitt, and R. X. Huang (1998), Sensitivity of GFDL Modular Ocean Model to parameterization of double-diffusive processes, *J. Phys. Oceanogr.*, *28*, 589–605.

M. S. Glessmer and A. Oschlies, IFM-GEOMAR, Leibniz Institute of Marine Sciences at Kiel University, Düsternbrooker Weg 20, D-24105 Kiel, Germany. (mglessmer@ifm-geomar.de; aoschlies@ifm-geomar.de)

A. Yool, National Oceanography Centre, Southampton; European Way, Southampton, Hampshire, SO14 3ZH, UK. (axy@noc.soton.ac.uk)